Received: 11 September 2023 | Revised: 26 March 2024 | Accepted: 18 May 2024

DOI: 10.1002/jbm.b.35434

RESEARCH ARTICLE

Calcium phosphate graphene and $Ti_3C_2T_x$ MXene scaffolds with osteogenic and antibacterial properties

Jason D. Orlando[1] | Li Li[1] | Tej B. Limbu[2,3] | Chenyun Deng[4] | Michelle E. Wolf[1] | Walker M. Vickery[1] | Fei Yan[3] | Stefanie A. Sydlik[1]

[1]Department of Chemistry, Carnegie Mellon University, Pittsburgh, Pennsylvania, USA

[2]Department of Physical and Applied Sciences, University of Houston-Clear Lake, Houston, Texas, USA

[3]Department of Chemistry and Biochemistry, North Carolina Central University, Durham, USA

[4]Department of Biomedical Engineering, Carnegie Mellon University, Pittsburgh, PA, USA

Correspondence
Stefanie A. Sydlik, Department of Chemistry, Carnegie Mellon University, 4400 Fifth Avenue Pittsburgh, PA, USA.
Email: ssydlik@andrew.cmu.edu

Abstract

Bioactive degradable scaffolds that facilitate bone healing while fighting off initial bacterial infection have the potential to change established strategies of dealing with traumatic bone injuries. To achieve this a composite material made from calcium phosphate graphene (CaPG), and MXene was synthesized. CaPG was created by functionalizing graphene oxide with phosphate groups in the presence of CaBr with a Lewis acid catalyst. Through this transformation, Ca^{2+} and PO_4^{3-} inducerons are released as the material degrades thereby aiding in the process of osteogenesis. The 2D MXene sheets, which have shown to have antibacterial properties, were made by etching the Al from a layered Ti_3AlC_2 (MAX phase) using HF. The hot-pressed scaffolds made of these materials were designed to combat the possibility of infection during initial surgery and failure of osteogenesis to occur. These two failure modes account for a large percentage of issues that can arise during the treatment of traumatic bone injuries. These scaffolds were able to retain induceron-eluting properties in various weight percentages and bring about osteogenesis with CaPG alone and 2 wt% MXene scaffolds demonstrating increased osteogenic activity as compared to no treatment. Additionally, added MXene provided antibacterial properties that could be seen at as little as 2 wt%. This CaPG and MXene composite provides a possible avenue for developing osteogenic, antibacterial materials for treating bone injuries.

KEYWORDS
antibacterial, functional graphenic material, graphene, MXene, osteoinductive

1 | INTRODUCTION

Traumatic bone injuries can present in many ways and require various treatment methods to remedy. Injuries that result in critical bone sized defects create an additional layer of complexity. This is because these injuries will not spontaneously heal on their own, even with surgical stabilization.[1] Generally, this label is applied to defects greater than 1–2 cm in length or greater than 50% circumference loss of the bone. However, it can be highly variable depending on location, the state of the soft tissue around it, and other characteristics of the patient and mechanism of injury.[1]

When spontaneous healing is not an option, the gold standard of treatment is an autogenous bone graft often accompanied by fixation.[2,3] In this approach, healthy bone is harvested from the patient, typically from the iliac crest, which can then be used to fill the injury site.[2–6] This graft aids in patient recovery due to its innate osteogenic

properties; however, they are not without risk. They can cause surgical site morbidity, and they increase the likelihood of further injury, infection, pain, and bleeding.[2,3] Additionally these techniques have an upper limit of bone loss to which they are viable including but not limited to location, patient health, and how much bone was lost.[7,8]

Autogenous bone grafts require fixation whenever load bearing or adhering bone pieces together is required. Internal fixation on traumatic bone injuries is accomplished using a combination of wires, screws, plates, interlocking nails, and pins.[9,10] The hardware seeks to stabilize the injury site during the healing process and possibly maintain range of motion or function depending on the specifics of the injury. Internal fixation can also be used with injuries that do not have critical bone loss. In these injuries, stabilization of the wound and alignment of the bone is all that is needed for healing to occur.[4,10]

Traditional orthopedic hardware is made of metals like stainless steel and titanium.[10] These metals are much stronger and stiffer than bone so under cyclic loading this difference can cause damage to the implant or injury site.[11] These prosthetics can lead to osteolysis, aseptic loosening, or additional patient pain over time.[12] This is especially problematic as internal hardware tends to be implanted with the intent that the hardware is permanent. Even interlocking nails, which see high success rates of bone union of up to 95%, still have complications.[9,10] One common issue is infection along the pin tracks of external stabilizing hardware. Even in traditional plate-based hardware, infection rates can be as high as 35%.[7,13] The infections at these sites tend to present as biofilms and as such are more difficult to treat.[14] Even in cases where proactive removal of internal hardware occurs after healing, there are still down sides to consider. Patients could experience refractures, infections, damage to soft tissue, and so forth, in addition to the extra surgery and recovery time associated with it.[11]

To bypass these negative side effects discussed, researchers have turned to biocompatible materials that degrade in the body. Using these bioresorbable materials negates the necessity of a second surgery to remove fixtures after the wound has healed. Hardware like plates, sutures, screws, pins, and more made of various bioresorbable materials have been utilized to treat patients.[15–17] These fixators reduce the risk associated with mechanical property mismatch that can occur from traditional hardware. Additionally, bioresorbable hardware can be tailored to release bioactive substances as they degrade.[17,18] These advantages make resorbable hardware an attractive option for treating traumatic bone injuries. However, bioresorbable materials lack the strength of traditional fixators, especially compared to metallic implants. This limits the use of bioresorbable materials in load bearing sites.[16,17]

Functional graphenic materials (FGMs) have potential as next generation orthopedic hardware because they are both bioresorbable and have a high degree of mechanical strength.[19,20] A common graphene-based derivative is graphene oxide (GO). GO has been used to improve the mechanical properties of other materials in composite bioresorbable scaffolds.[21,22] The presence of carboxyl, epoxide, and hydroxyl groups on GO allow it to be more dispersible in water than pristine graphene by providing functional handles to attach useful biomolecules.[19,22,23] Additionally, reduced GO (rGO) has been shown to promote osteogenic differentiation when used as a coating, allowing the implant to be loaded with bioactive molecules that further increased osteogenic activity.[19,22–24] Bioresorbable materials like collagen and chitosan have also been coated or blended with graphenic materials to increase mechanical properties as well as bioactivity.[21,22]

The need for mechanically strong, osteoinductive, bioresorbable orthopedic hardware was the driving force for the creation of calcium phosphate graphene (CaPG). CaPG is GO that has been functionalized with polyphosphate and calcium ions by an Arbuzov reaction. These chemical modifications to the material allows for the release of Ca^{2+} and PO_4^{3-} ions upon biosorption of the material. These inducerons can then go on to induce osteogenesis as the material breaks down in the body.[25] In vitro, CaPG was shown to be intrinsically osteoinductive and induced osteogenesis in human mesenchymal stem cells (hMSCs) to the same extent as media containing known osteogenic growth factors.[25]

Despite promising reports in vitro and in vivo, further work must be conducted to create a functional scaffold comprised of CaPG. While CaPG meets the criteria of a bone mimetic scaffold, it lacks antibacterial properties. MXene and MXene based conjugates have shown to possess antibacterial, anti-biofouling properties, and guided bone regeneration.[26–33] MXenes are a class of inorganic 2D materials comprised of layered transition metal carbonitrides. Specifically, titanium carbide MXene ($Ti_3C_2T_x$ where T_x represents O, OH, F terminations on the MXene)[30,32,34–36] was added to create a composite material with CaPG. Research suggests these properties are a result of the sharp edges of the material and the oxidative stress it causes on the membranes of bacteria.[29–31,33] By incorporating MXenes in a CaPG scaffold, we aim to design an osteogenic bone scaffold with inherent antibacterial capabilities.

2 | METHODS AND MATERIALS

2.1 | Synthesis of CaPG

To synthesize CaPG first GO had to be made. GO was made through a modified Hummer's method. A 10 g graphite flakes (graphite flake, natural, −325 mesh, 99.8% metal basis; Alfa Aesar, Ward Hill, MA, USA) was added to a 4 L flask containing 250 mL concentrated sulfuric acid chilled over ice. Afterwards, 20 g of $KMnO_4$ (99.0% crystalline, Alfa Aesar) was added over 20–30 min. Then the reaction was warmed to room temperature to stir for 2 h, followed by heating to 35°C to stir for 2 h more. Heat was removed, and the reaction was quenched by adding 1400 mL DI water, 20 mL 30% H_2O_2 (VWR), and 450 mL more DI water. The reaction was left to stir overnight. Afterwards the reaction was vacuum filtered to isolate the GO, which was loaded into 3500 molecular weight cutoff dialysis tubing (SnakeSkinTM dialysis tubing; Thermo Scientific) to dialyze against water for 7 days with DI water changed twice a day. Finally, the GO was frozen at −80°C and lyophilized for 3 days till dry.

To synthesize CaPG, 2 g of prepared GO, 500 mL triethyl phosphite (Sigma Aldrich), and 2 g magnesium bromide diethyl etherate (Alfa Aesar) were put into a flame-dried round-bottom flask under nitrogen gas. The reaction mixture was sonicated for an hour, after which 10 g of CaBr (Alfa Aesar) was added to the mixture under nitrogen gas and sonicated for 30 min. The round bottom was then refluxed at 156°C under nitrogen gas for 72 h with vigorous stirring. The CaPG was then removed from the mixture via vacuum filtration. The isolate was washed via centrifugation at 3600*g* for 10 min twice with acetone, once with DI water, once with ethanol and twice more with acetone. The isolated CaPG was dried under vacuum for 48 h.

2.2 | MXene synthesis

Synthesis of MXene started with the Al etching of Ti_3AlC_2 MAX phase from Carbon-Ukraine as detailed in the previous report.[37] MAX phase powder (0.5 g) was slowly added to 10 mL of 30% hydrofluoric acid (Acros Organic) under constant stirring for 7 h. The solution was cleaned via centrifugation at 3500 rpm for 30 min, and the supernatant was removed. The isolate was then washed with 5 L of DI water via vacuum assisted filtration until the pH was lowered to about 6.5. The MXene was then dried for 1 day in a vacuum desiccator, after which the delamination process was carried out by mixing 0.1 g of MXene powder with 50 mL of 25 mM tetrabutylammonium hydroxide (TBAOH) (Alfa Aesar, Electronic grade, 99.9999% (metal basis) liquid) and was shaken for 48 h. The solution was centrifuged several times at 5000 rpm for 30 min until the pH of the solution was approximately 7. The MXene was then centrifuged at 3500 rpm for 5 min to separate off the MXene that was not delaminated and unetched MAX phase from the colloidal delaminated MXene.

2.3 | Hot-pressed pellet formation

To form the hot-pressed pellets 10 mg of sample with the desired weight ratio was weighed out. The powder was then loaded into a cylindrical mold with a 4 mm inner diameter that had been heated to 200°C. The pellet was then formed by putting the mold in a vice with applied pressure for 60 s. The formed pellet was then weighed again for a final pellet weight. After pressing all the pellets, they were heat treated at 200°C for 20 min, which resulted in the final pellet products required for further testing.

2.4 | Elution studies

To test for the elution of Ca and phosphate the Piper phosphate, and calcium o–cresolphthalein complexone assay were utilized, respectively. For each assay, standards were made, and standard curves were calculated according to the manufacturer's specifications.[38–41] Then, 10 mL of 1 molar Tris buffer solution was poured into sealed 20 mL reaction vials, which each contained the pellet to be studied. According to desired time points, aliquots were removed from the solution adjacent to the pellet via micropipette being careful not to disturb or damage the pellet. In the case of the Piper phosphate assay, 50 µL aliquots were taken and for the calcium o–cresolphthalein complexone assay. These aliquots were placed into a labeled 96 well plate. After all time plates were taken the respective assay could be run to determine the concentration of the ions of interest, by using the standard curve constructed earlier.

2.5 | Antibacterial experiments

Mueller Hinton broth was made by dissolving 11 g of cation adjusted BBL Mueller Hinton II dehydrate in 500 mL of DI water for a final media concentration of 3.0 g/L beef extract, 17.5 g/L acid hydrolysate of casein, 1.5 g/L starch, 25 mg/L calcium, and 12.5 mg/L magnesium. The broth was autoclaved at 121°C for 30 min and then cooled to room temperature prior to use. *E. coli* strain K12 (ATCC 25404TM) was kept as a frozen stock (−80°C) in bacterial culture media with 30% glycerol. To prepare the inoculum, frozen bacterial stocks were thawed, then centrifuged at 10,000 g for 10 min. The media was aspirated, and the bacteria pellet was redispersed in 5 mL of fresh broth. The liquid culture was incubated with rotational shaking for 16 h at 37°C. The bacteria culture was centrifuged at 10,000 g for 10 min to pellet the cells followed by aspiration of the supernatant and resuspension of the pellet into 5 mL of fresh broth. Cultures were then diluted with a 1:5 ratio (1 mL stock cell suspension and 4 mL fresh broth). The solution was then further diluted with broth to give a 4% v/v solution of the 1:5 split. The 4% v/v solution of 1:5 split (which had a concentration of $3.5*10^8$ CFU/mL) was used as the inoculum for experiments involving coculture of bacteria with the pellets.

2.6 | In vitro cell experiments

2.6.1 | Cell culture

NIH–3 T3 murine fibroblasts and RAW 264.7 murine macrophages were cultured in Dulbecco's Modified Eagle Medium with 4500 mg/L D–glucose, 584 mg/L L–glutamine, and 100 mg/L sodium pyruvate (ThermoFisher, catalog #11995065). This basal media was supplemented with 10% v/v calf serum (ThermoFisher, catalog #16010159) for NIH-3 T3 cells and 10% v/v fetal bovine serum (ThermoFisher, catalog #26140079) for RAW 264.7 cells. Both medias were also supplemented with penicillin streptomycin antibiotics (ThermoFisher, catalog #15140122) that was diluted to a final concentration of 100 U/mL. The cells were cultured in an incubator at 37°C with a humidified atmosphere at 5% CO_2.

2.6.2 | Cytocompatibility of MXene

Cytocompatibility of the pure MXene material was assessed by exposure of two mammalian cell lines to dispersions of different concentrations of the powder. Powders were sterilized via 10 min of 254 nm

ultraviolet light exposure in microcentrifuge tubes, and stock solutions of 600 μg/mL were prepared and sonicated for 10 min. NIH–3 T3 fibroblasts and RAW 264.7 macrophages were seeded in the interior wells of 96–well plates at a density of at 3×10^4 and 2×10^4 cells/cm^2, respectively. After 2 h, the cells were considered well-adhered. The media was aspirated and replaced with appropriate volumes of new media and MXene stock solutions to achieve final volumes of 200 μL and the desired concentrations of 1, 10, and 100 μg/mL of MXene. A no treatment condition of just media was included for comparison as well. Cells were allowed to grow in the incubator for 48 h, and then the vitality assays were performed. Cellular enumeration, vitality, and late necrosis and apoptosis was assessed using fluorescent reporters. The media and materials were aspirated from the wells, and the following fluorescent staining solution was added: PBS (ThermoFisher, catalog #10010023) with 20 μM of Hoechst 33342 (ThermoFisher, catalog #62249) 2.5 μM of Calcein AM (ThermoFisher, catalog #C3099), and 1.5 μM of propidium iodide (Alfa Aesar, catalog #J66584-AB). After 10 min in the incubator, the staining solution was aspirated and replaced with PBS. A microplate reader was used to measure fluorescent signals.

2.6.3 | Mesenchymal stem cell experimental set-up

CaPG scaffolds with 0%, 2%, 10%, 20%, and 40% MXene by weight were transferred into a biosafety cabinet and exposed to UV light for 5 min. The scaffolds were further sterilized by soaking in 70% ethanol for 10–15 min in petri dishes. The ethanol was aspirated, and the scaffolds were soaked in PBS for 10–15 min, followed by aspiration and another 10–15 min soak in PBS. The scaffolds were then transferred to individual wells on tissue culture-treated 96-well plates. Separate plates for each time point for each experiment were used, with three scaffolds of each material for alkaline phosphatase assay and one scaffold of each material for fluorescent imaging. Bone marrow-derived human mesenchymal stem cells (RoosterBio, passage number 2) were grown to confluency in a T25 tissue culture flask in mesenchymal stem cell growth media consisting of MesenPRO RS Basal Medium with 2% MesenPRO RS Growth Supplement (ThermoFisher, catalog #12746012), 2 mM of L-glutamine (ThermoFisher, catalog #A2916801), and 100 μg/mL of penicillin–streptomycin (ThermoFisher catalog #15140163). The cells were washed with cold PBS (ThermoFisher, catalog #10010023), trypsinized with TrypLE Express dissociation reagent (ThermoFisher, catalog #12604013), pelleted, and resuspended in growth media at an approximate density of 2000 cells/μL. 0.4% Trypan blue stain (ThermoFisher, catalog #T10282) and a hemocytometer slide (Funakoshi, 4-chamber disposable slides) were used to compute the live cell density, and this result was used to adjust the resuspension volume to achieve a density of 1000 cells/μL. A 10 μL of the cell suspension was pipetted onto each scaffold (or pipetted directly onto the well plate for no treatment and osteogenic positive control conditions). The well plates were transferred to the incubator, and after 1 h, 200 μL of equilibrated media was carefully in each well. Growth media was used for all treatment conditions except osteogenic positive control, which received osteogenic media consisting of StemPRO Osteocyte/Chondrocyte Differentiation Basal Medium with 10% StemPRO Osteogenesis Supplement (ThermoFisher, catalog #A1007201) and 5 μg/mL gentamicin sulfate (ThermoFisher, catalog #15710064). Old media was aspirated and replaced with freshly prepared media on day 14 for remaining well plates after this time point.

2.6.4 | Alkaline phosphatase assay

The SensoLyte pNPP Alkaline Phosphatase Assay Kit Colorimetric from AnaSpec (catalog #AS-72146) was used for quantitative measurement of alkaline phosphatase levels in the samples. 1X assay buffer was prepared by diluting the 10X assay buffer with deionized (DI) water. A standard curve was produced using the provided ALP standard. The standard (10 μg/mL) was diluted 1:50 in 1X assay buffer to achieve a 0.2 μg/mL (200 ng/mL) concentration. Serial dilutions were performed to achieve 100, 50, 25, 12.5, 6.25, 3.125, 1.5625, 0.78125 ng/mL concentrations, and these solutions were added to wells of a 96 well plate in triplicate with a 50 μL volume. A 50 μL of p-nitrophenyl phosphate (pNPP) solution was added to each well, and the plate was gently shaken for 30 s. After 45 min at room temperature, 50 μL of stop solution was added to each well. The absorbance at 405 nm was measured and plotted against ALP concentration. A best fit linear line was generated.

0.2% Triton X-100 lysis buffer was prepared by adding 5 μL Triton X-100 to 2.5 mL 1X assay buffer, and vortexed to mix. On days 1, 7, 14, and 21 of the experiment, the appropriate plate was removed from the incubator for the ALP assay. Media was aspirated and wells were washed twice with 100 μL of 1X assay buffer. A 50 μL lysis buffer was added to each well, and the plate was incubated at 4°C for 10 min. The plate was sealed with parafilm and sonicated for 4 min, taking care to keep the water level below the top of the wells. The plate was dried off and incubated at −20°C for 10 min. The liquid was aspirated from each well, transferred to separate 0.2 mL microcentrifuge tubes, and centrifuged at 2500 × g and 4°C for 10 min. The supernatant was aspirated from each tube, taking care to avoid the debris pelleted at the bottom, and was transferred into new wells on the 96 well plate. A 50 μL pNPP solution was added to each well, and the plate was gently shaken for 30 s. After 45 min at room temperature, 50 μL stop solution was added into each well. The absorbance at 405 nm was measured, and the best fit line was used to convert absorbance to a concentration of ALP in the samples.

2.6.5 | Fluorescent imaging

The fixative solution was prepared by diluting 37% formaldehyde (Alfa Aesar, catalog #A16163) in DI water to 4%. The fluorescent staining solution was prepared by adding Hoechst 33342 (ThermoFisher, catalog #62249) and Alexa Fluor 488 Phalloidin (ThermoFisher, catalog #A12379) to PBS at concentrations of 40 μM

and 66 μM, respectively. The Alexa Fluor 488 Phalloidin had previously been dissolved in methanol (Fisher Chemical, catalog #A452-4) to produce a 40X stock solution. On days 1, 7, 14, and 21 of the experiment, the appropriate plate was removed from the incubator for fixing and fluorescent staining. Media was aspirated, and the wells were washed with PBS 3 times. The plate was moved to a chemical fume hood. The wells were incubated in 100 μL of fixative solution for 10–15 min, and then twice in 100 μL of PBS for 10–15 min. A 100 μL of fluorescent staining solution was added to each well and the plate was protected from light for 1–2 h during the incubation. The wells were washed once more with 100 μL of PBS for 5–10 min. The scaffolds were then flipped upside down with tweezers and imaged with a microscope on DAPI and GFP fluorescent light channels.

2.7 | Statistical analysis

Statistical significance was carried out using a *T* test with each *p* value listed in the figure description. High resolution XPS scans were analyzed using Fityk fitting software. Percentages of each shift in XPS was determined by peak integration. Bacterial viability data were generated using fluorometry data from the LIVE/DEAD™ BacLight™ Bacterial Viability assay.

3 | RESULTS

CaPG was created by a Lewis acid-catalyzed Arbuzov reaction on epoxides in the synthesized GO.[25] MXenes were prepared through top-down etching and delamination of MAX phase bulk crystals.[36] Varying weight ratios were explored to determine the structure property relationships of the composite.

To create a CaPG MXene composite, bulk mixtures of powders were hot pressed into pellets. This preparation technique was chosen for its ease, cost effectiveness, and relatively mild conditions. TGA indicated that both MXene and CaPG were stable at temperatures beyond 200°C (Figure S1). Thus, CaPG and MXene were hot-pressed at 200°C for 1 min into 4 mm diameter pellets followed by heat treatment at 200°C for 20 min. These pellets were used for all further experiments. SEM images using the backscatter electron (BSE) detector can be seen in Figure 1. These qualitatively show the various pellets at different weight percentages of MXene as the BSE detector can be used to draw stark distinctions between atomic size.

Changes in atomic composition and bonding of the pellets upon hot-pressing were assessed using XPS. Survey scans revealed that atomic composition of both CaPG and MXene minimally changed post-processing into pellet form, with non-significant change in oxygen content in both materials (Figure S2). High resolution measurement revealed minimal changes in CaPG as well (Figure S3). Conversely, noticeable changes were observed in MXene after pellet pressing, with the Ti2p peaks demonstrating that titanium is being oxidized (Figure 2). This is supported by the fact that the higher oxidation state of Ti^{4+} is much more prevalent after hot pressing the sample.[36] Additionally, the C1s peaks show that the carbon–oxygen bonds decrease relative to the carbon–carbon bonds. Combined with the minimal change in the survey scans, this suggests oxygen preferentially moves from carbon to titanium under heat and pressure. Since prior research has demonstrated that oxidized MXenes are more antibacterial,[29] this oxidation could be beneficial for the bactericidal properties of the pellet.

Pellets of CaPG and MXene with varying compositions were tested for antibacterial activity. It was hypothesized that the antibacterial mechanism of action would be due to sharp edge interactions of the MXene material and the generation of radical oxygen species.[27–30] Both interactions are expected to occur at the surface of the material rather than proliferate throughout the solution. Therefore, antibacterial properties were measured at the surface and in solution to confirm the mechanism of action. To test the viability of cells in solution with pellets both BacLight fluorescence assay and plate counting post dilution were employed. These tests showed that the presence of pellets regardless of weight percent MXene had virtually no impact on *E. coli* proliferation in solution (Figure S4). Both methods showed that even at 100% MXene, bacteria were unaffected as compared to the no treatment conditions. To test the viability of *E. coli* at the surface of these pellets (0%, 50%, and 100% MXene) fluorescent dyes were used to stain the bacteria that had adhered to the top of the pellets during bacterial proliferation. This assay showed bacteria viability is much lower on pellets that contain MXene versus CaPG and that 50% MXene and 100% MXene pellets have similar performance

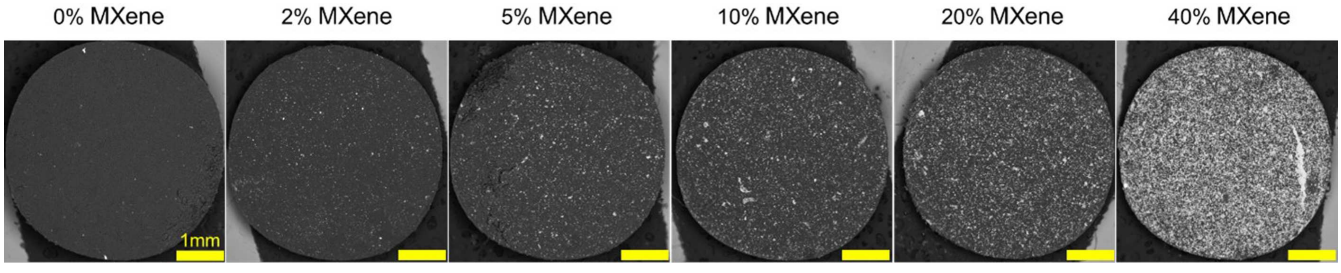

FIGURE 1 Whole pellet SEM images with varying concentrations of MXene relative to CaPG using the SEM backscatter electron (BSE) detector to show qualitatively the incorporation of MXene into the pellets. Lighter regions correspond to heavier elements, in this case titanium, which is present only in the MXene component.

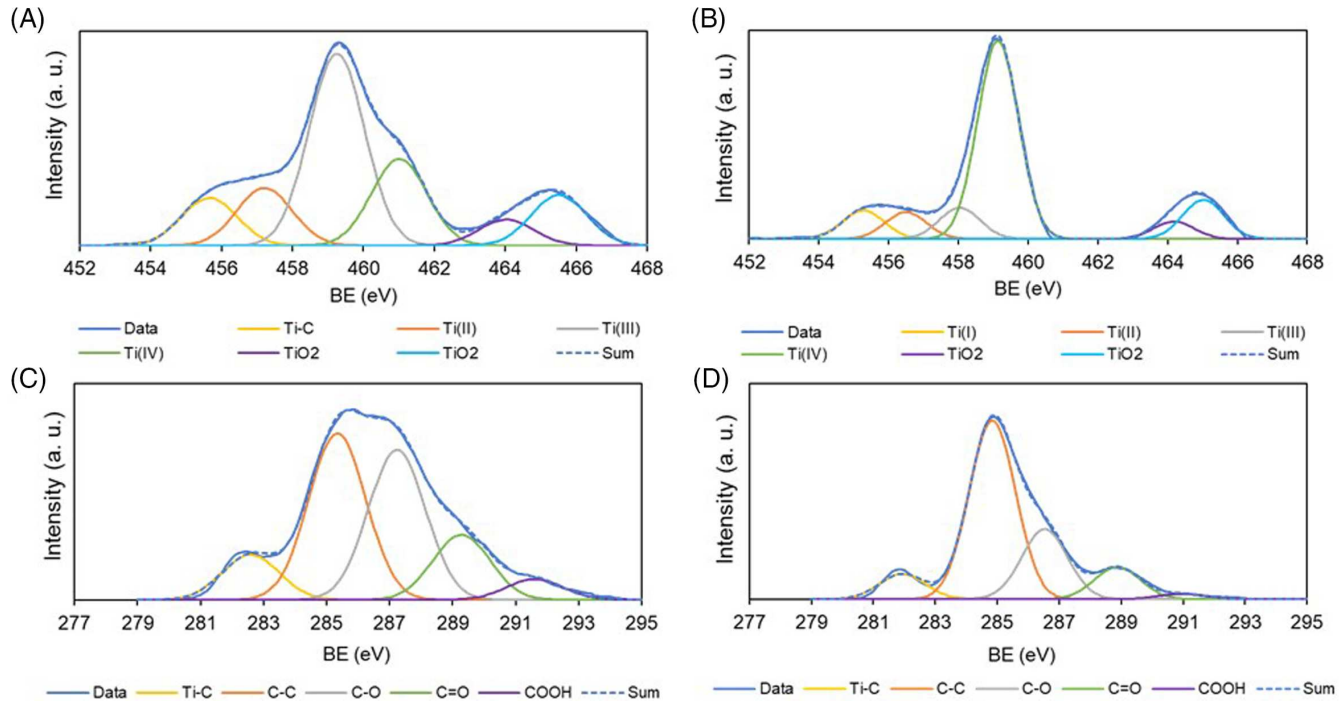

FIGURE 2 (A) and (B) are the Ti2p for MXene powder and pellet, respectively. (C) is the C1s spectrum for MXene powder whereas (D) is the C1s for MXene pellet.

(Figure S4). Based on these results, additional bacterial studies were done to determine the impact below 50% MXene.

Increasing content of MXene resulted in lowered bacterial cell viability, confirming antimicrobial activity (Figure 3A,B). The data suggest that initial increases in MXene content have the largest impacts on bacteria proliferation (Figure 3B). Even pellets with 0% had an impact on bacterial viability, which was increased at even just 2% loading of MXene. Additionally, it was observed that larger MXene weight percentages (≥ 20%) resulted in fewer bacteria adhered on the pellet surface (Figure 3C). A possible cause for this phenomenon may be the surface charge of MXene versus CaPG, as MXene has a more negative surface potential than CaPG (Figure S5).[42,43] The presence of both the antibacterial as well as antifouling properties observed with differing MXene weight percentages allow for tunability in the desired application.

The use of CaPG for guided bone regeneration is particularly useful as it has been shown to be both osteoinductive and osteoconductive due to release of inducerons as it degrades.[25] The goal of the composite material is to take advantage of these properties of CaPG while gaining the antibacterial properties displayed by MXene. Ion assays on the pellets of various weight percentages of MXene were carried out to see the impact of CaPG reduction on the ability to elute inducerons.

To study the elution of phosphate ions, the piper phosphate assay was utilized (Figure 4A). The phosphate release data revealed that incorporation of MXene did not affect the ability of the CaPG to elute phosphate: a relatively constant elution of PO^{4-} was observed with no clear trend resulting from MXene incorporation. To evaluate the elution of calcium, the o–cresolphthalein complexone assay was used (Figure 4B). Conversely, the calcium assay showed a clear trend: incorporation of greater amounts of CaPG resulted in greater Ca^{2+} elution. Statistically significant results at day 28 were observed for all pairings except for 0 and 2 wt %, and 2 and 10 wt %. However, both components elute from the CaPG, there is a clear difference in how these two ions are released. The calcium is ionically bound to the CaPG; thus, it is expected that these ions would be more willing to dissociate in solution over this time frame. On the contrary, phosphate groups of CaPG are covalently bound to the GO backbone. This difference results in the release profiles observed. Hot pressed pellet morphology allows only the outside layers to participate in the release of ions into solution, which would not be the case in more porous scaffolds.

To evaluate cytocompatibility of the pure MXene material, two mammalian cell lines were exposed to varying concentrations of MXene as a dispersion in cell media. NIH-3 T3 fibroblasts and RAW 264.7 macrophages were chosen as these cell types are representative of an initial foreign body response, such as to a biodegradable bone implant. The cells had good vitality, near 100%, in all treatment groups (Figure S7). The highest concentration of MXene yielded a statistically significant reduction in fibroblast vitality (64%); however, 100 μg/mL is a larger concentration than these cells would realistically experience in vivo as the MXene would only be used as a small weight fraction (less than 10%) additive in a scaffold. This data suggests that MXene is relatively safe for biological applications.

CaPG scaffolds with varying weight percentages of MXene were assessed for their ability to induce osteogenesis in vitro. To accomplish this, bone marrow-derived mesenchymal stem cells were seeded

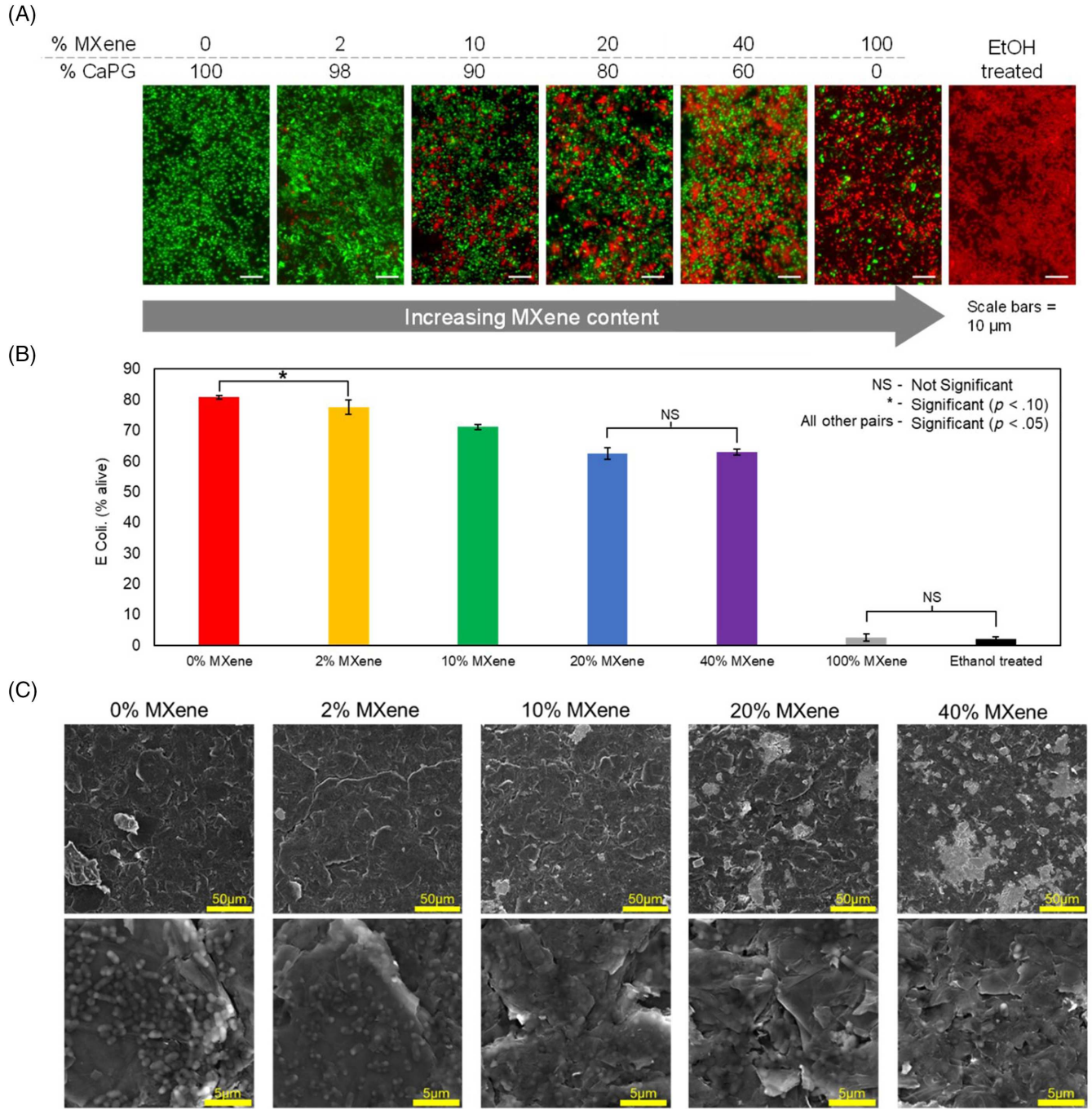

FIGURE 3 Proliferation of *E. coli* cells on the surface of CaPG/MXene pellets with varying weight percentages of MXene with an ethanol treated CaPG pellet as a positive control for 100% cell death. (A) Optical images of the pellet surfaces were collected to show green fluorescent dye representing live cells (Syto 9) and red fluorescent dye representing dying cells (propidium iodide) to access antibacterial efficacy. The assay allowed for the quantification of intensity of each dye to establish a percent live for *E. coli* on each pellet type (B). Pellets of each type were not stained following bacteria growth and instead were fixed to their respected pellet surfaces so that they could be imaged via SEM (C).

on scaffolds with 0, 2, 10, 20, and 40 wt % MXene and incubated for 21 days. Controls of cells on a well plate surface (no treatment) and cells on a well plate surface with osteogenic media (positive control) were included for comparison. At days 1, 7, 14, and 21, an alkaline phosphatase assay and fluorescent staining and imaging was performed. Alkaline phosphatase is a known osteogenic marker and can readily be measured via colorimetric assay. Total alkaline phosphatase (intracellular and secreted) was measured because secreted protein may adsorb to the scaffold surface and is difficult to reliably isolate. The treatment groups of 0 and 2 wt% MXene were found to support osteogenesis. Pellets with 0 wt% yielded statistically greater alkaline phosphatase levels than no treatment at day 14 and day 21, while 2 wt% showed statistically greater alkaline phosphate levels at day 21 (Figure 5A). Nuclei and actin stains were used to visualize cell

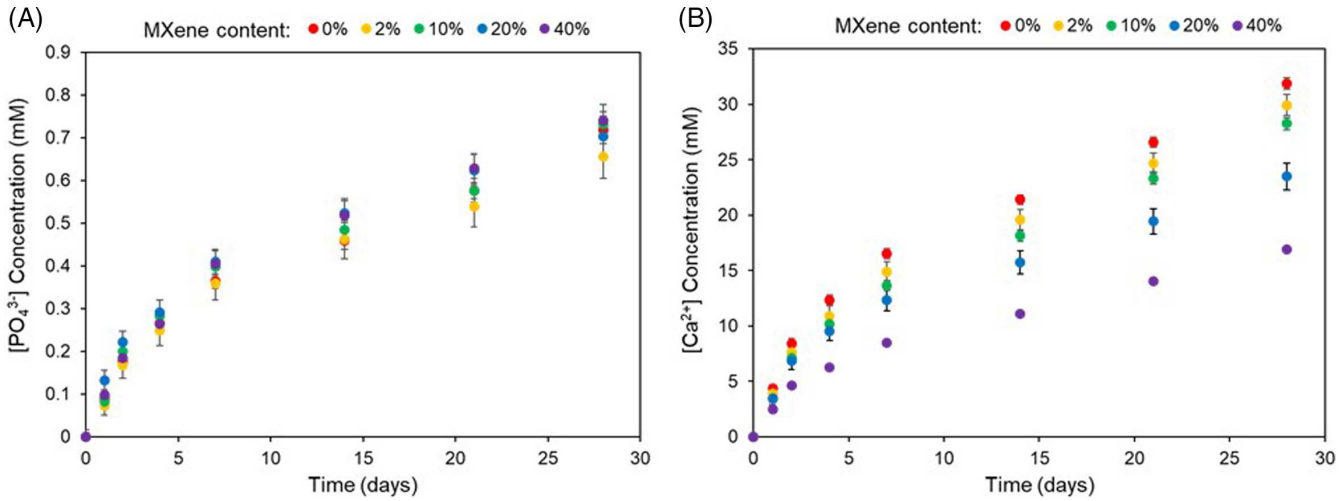

FIGURE 4 (A) Depicts the results of the Piper phosphate assay on pellets submerged in tris buffer (pH 7.2) with varying weight percent of MXene. At day 28, all scaffolds were not statistically significant from one another ($p < .05$). (B) Shows the results of the calcium o–cresolphthalein complexone assay on pellets of varying weight percentages submerged in tris buffer. Ca concentration was statistically significant at day 28 except for 0 and 2 wt%, and 2 and 10 wt%.

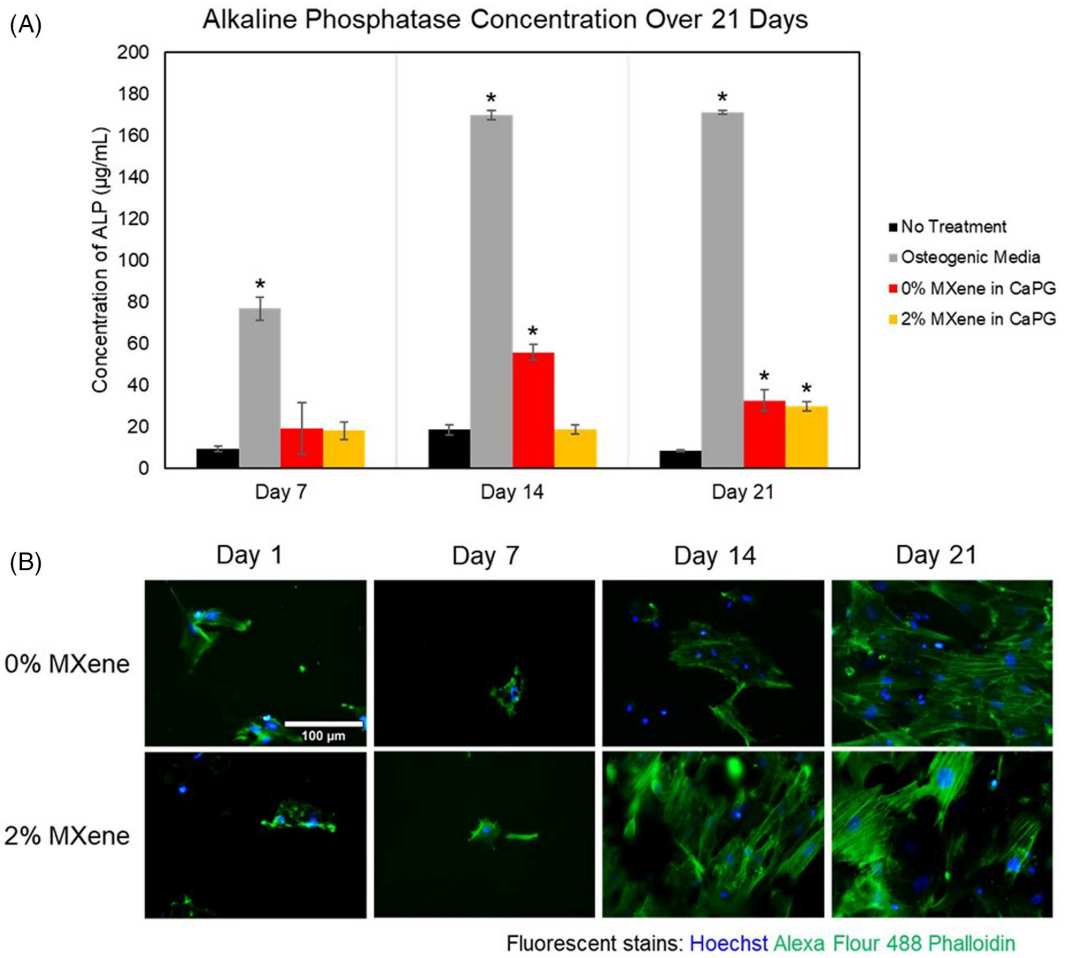

FIGURE 5 Osteogenic differentiation of mesenchymal stem cells on MXene/CaPG pellets. (A) Alkaline phosphatase (ALP) levels at days 7, 14, and 21 for no treatment (well plate surface), positive control of well plate surface with osteogenic media, CaPG pellet with no MXene, and CaPG pellet with 2 wt% MXene. Asterisk (*) indicates statistical significance from no treatment for each time point ($p < .1$). (B) Representative fluorescent images at days 1, 7, 14, and 21 for pellet treatment groups. Fluorescent stains include Hoechst, which stains nuclei, and Alexa Fluor 488 Phalloidin, which stains F-Actin (a cytoskeleton protein).

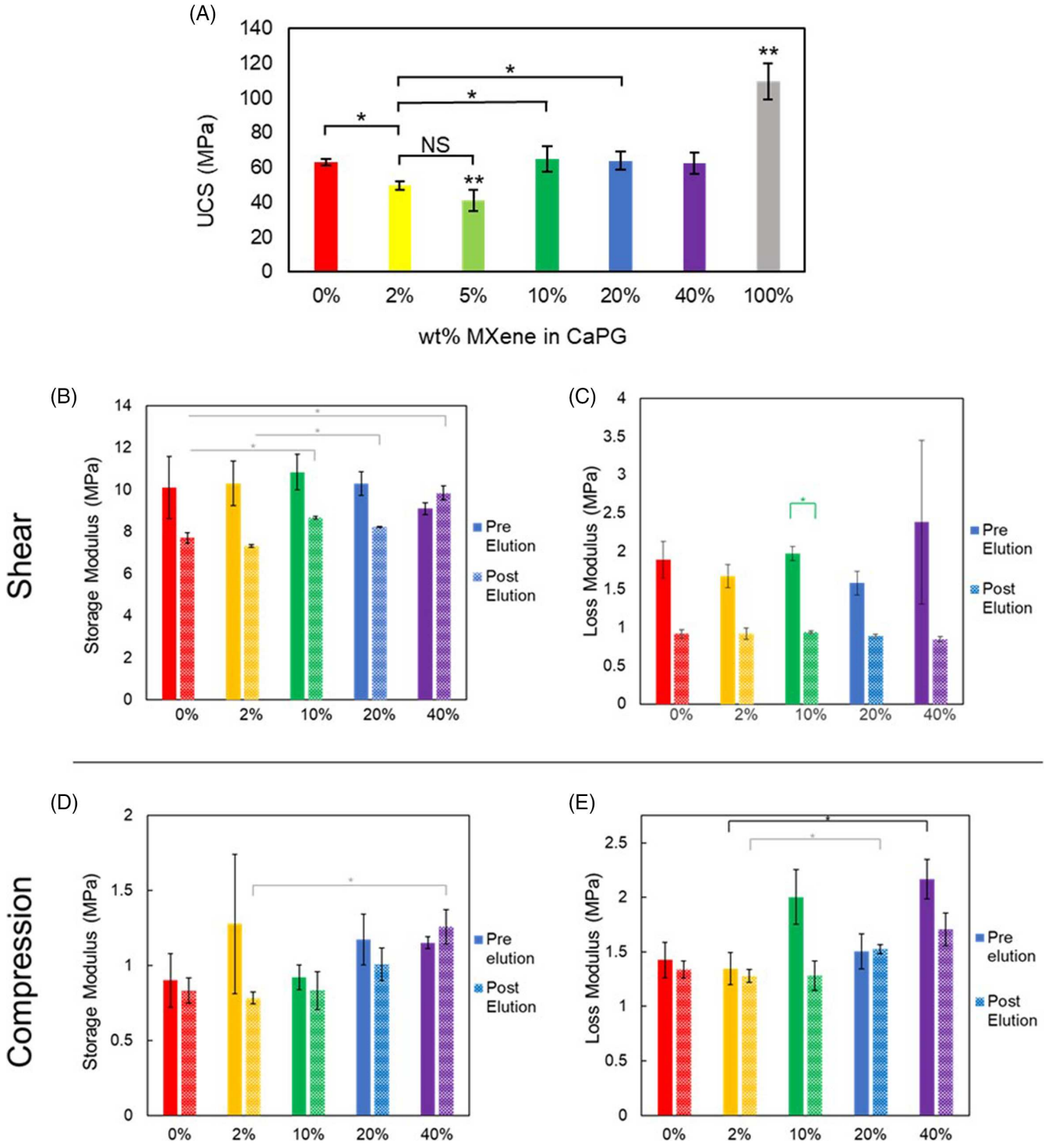

FIGURE 6 Mechanical properties were measured for pellets. The mechanical properties were measured a second time of the pellets after being freeze dried following the ion elution assays. The ultimate compressive strength (A), oscillatory shear (B & C) and oscillatory compression (D & E) measurements were taken with a pre-force of 1 N and a frequency of 1 Hz. Open ended brackets denote statistical significance (p value <.05, pre-elution in black, post-elution in gray) between the bracketed sample and all others of that type beneath the bracket. Double asterisks indicate statistical significance between all other samples unless otherwise stated.

morphology in fluorescent imaging. On 0 and 2 wt% MXene scaffolds, it is observed that cells show significant F-actin fiber development and alignment at days 14 and 21 (Figure 5B), which is a morphology associated with osteogenic differentiation.[44] Scaffolds with 10, 20, and 40 wt% MXene content were not found to support osteogenesis with negligible alkaline phosphatase levels and no cell morphology

changes. In conclusion, 2 wt % MXene as an additive in CaPG scaffolds was compatible with osteogenic CaPG.

Mechanical properties that can mimic that of bone are desirable but are difficult for bioresorbable materials to achieve. Cortical bone has an average longitudinal ultimate compressive strength of 199 MPa.[45] Especially for load bearing orthopedic hardware, closely approximating this value will be necessary. Thus, the ultimate compressive strength (UCS) of the pellets was tested. In addition, to shear and compression frequency sweeps of the as prepared pellets and after elution studies to see how composition and time in PBS affects mechanical properties.

The UCS of the materials showed that CaPG with added MXene did not significantly change its compressive strength except for 2% and 5%. CaPG samples with 2% and 5% MXene saw a small significant decrease in compressive strength. Pure MXene pellets had a significantly higher compressive strength at around twice that of the other scaffolds. It is believed that the smaller concentrations of MXene saw a decrease in compressive strength as the amount of MXene was low enough where pellets had biphasic compositions, which presented as failure points within the scaffolds. These materials prepared as hot-pressed pellets displayed around half or one third of the compressive longitudinal strength in cortical bone with the exception of pure MXene, which was much stronger.[45] However, these materials did display strength similar to that of widely used bone cements.[46,47]

MXene weight percentage did impact the shear mechanical properties of CaPG composites (Figure 6A,B). In general, the shear storage modulus was greater after elution with increasing MXene (Figure 6A). This is likely due to MXene breaking down more slowly than CaPG throughout elution, allowing it to maintain its storage modulus to a higher degree. This hypothesis is supported by SEM images of the pellets over the course of the elution period (Figure S6). In these images, the pellets with higher percent CaPG have rougher surfaces than those with higher weight percent MXene after 4 weeks of elution time in buffer.

Conversely, elution did not have an impact on compressive strength to a significant degree. Generally, samples had similar performance after elution as before with a slight trend toward higher MXene content resulting in larger storage and loss modulus (Figure 6C,D). Combined with the other data, this suggests that CaPG is largely degrading at the surface. As such, the integrity of the pellet under compressive strain is not significantly impacted compared to shear. This hybrid material exhibits a composition-dependent retention of shear storage modulus in mechanical properties over time with increasing MXene content.

4 | CONCLUSIONS

Antibacterial surface properties were successfully added to CaPG pellets through incorporation of MXene. Significant antibacterial activity was demonstrated with even relatively low concentrations (less than 10%) of MXene in the total pellet. Mechanical properties of this composite material were enhanced through the addition of MXene. These MXene-CaPG hybrid pellets eluted inducerons as they degraded, as with neat CaPG pellets. The release of phosphate was minimally impacted by the addition of MXene to the CaPG material. Calcium elution, however, was reduced equivalently to the percentage MXene present: 40 wt % MXene pellets had about a 40% reduction in calcium elution as compared to CaPG alone. Additionally, pellets made with 2 wt % MXene and CaPG alone equivalently induced osteogenesis in mesenchymal stem cells.

This work shows that CaPG can function with additives, allowing for incorporation of new desired properties while maintaining mechanical strength and osteogenic ability. Specifically, the MXene additive used can be imparted into a CaPG scaffold to give the material antibacterial properties. Due to the prevalence of bacterial infections in traumatic bone injuries, the ability to incorporate antibacterial activity into CaPG makes it an even more promising platform for bone regenerative applications.

ACKNOWLEDGMENTS

This work was supported by Sydlik's NIH R21 grant through the NIDCR (R21 DE029316). F. Y. thanks the financial support by the U.S. National Science Foundation (#2122044). T. L. thanks University of Houston-Clear Lake for funding (FRSF Award number A09S22). We thank J. Gillespie for providing training and use of the XPS (Materials Characterization Laboratory at the University of Pittsburgh). The authors acknowledge use of the Materials Characterization Facility at Carnegie Mellon University supported by grant MCF-677785.

DATA AVAILABILITY STATEMENT

The data that support the findings of this study are available from the corresponding author upon reasonable request.

ORCID

Fei Yan https://orcid.org/0000-0001-5983-143X
Stefanie A. Sydlik https://orcid.org/0000-0001-9375-2356

REFERENCES

1. Nauth A, Schemitsch E, Norris B, Nollin Z, Watson JT. Critical-size bone defects: is there a consensus for diagnosis and treatment? *J Orthop Trauma*. 2018;32:S7-S11.
2. Myeroff C, Archdeacon M. Autogenous Bone Graft: Donor Sites and Techniques. *J Bone Joint Surg Am*. 2011;93:2227-2236.
3. Schmidt AH. Autologous bone graft: is it still the gold standard? *Injury*. 2021;52:S18-S22.
4. Keating JF, Simpson AHRW, Robinson CM. The management of fractures with bone loss. *J Bone Joint Surg Br*. 2005;87-B:142-150.
5. Misch CM. Autogenous bone: is it still the gold standard? *Implant Dent*. 2010;19:361.
6. Sakkas A, Wilde F, Heufelder M, Winter K, Schramm A. Autogenous bone grafts in oral implantology—is it still a "gold standard"? A consecutive review of 279 patients with 456 clinical procedures. *Int J Implant Dent*. 2017;3:23.
7. El-Rosasy MA. Acute shortening and re-lengthening in the management of bone and soft-tissue loss in complicated fractures of the tibia. *J Bone Joint Surg Br*. 2007;89(1):80-88.
8. Betz AM, Hierner R, Baumgart R, et al. Primary shortening—secondary lengthening. A new treatment concept for reconstruction of extensive

soft tissue and bone injuries after 3rd degree open fracture and amputation of the lower leg. *Handchir Mikrochir Plast Chir*. 1998;30:30-39.
9. Stiffler KS. Internal fracture fixation. *Clin Tech Small Anim Pract*. 2004;19:105-113.
10. Taljanovic MS, Jones MD, Ruth JT, Benjamin JB, Sheppard JE, Hunter TB. Fracture Fixation. *Radiographics*. 2003;23:1569-1590.
11. Slone RM, Heare MM, Vander Griend RA, Montgomery WJ. Orthopedic fixation devices. *Radiographics*. 1991;11:823-847.
12. Skalak R. Biomechanical considerations in osseointegrated prostheses. *J Prosthet Dent*. 1983;49:843-848.
13. Stannard JP, Finkemeier CG, Lee J, Kregor PJ. Utilization of the less-invasive stabilization system internal fixator for open fractures of the proximal tibia: A multi-center evaluation. *Indian J Orthop*. 2008;42:426-430.
14. Trampuz A, Zimmerli W. Diagnosis and treatment of infections associated with fracture-fixation devices. *Injury*. 2006;37:S59-S66.
15. Pina S, Ferreira JMF. Bioresorbable plates and screws for clinical applications: A review. *J Health Eng*. 2012;3:243-260.
16. Sheikh Z, Najeeb S, Khurshid Z, Verma V, Rashid H, Glogauer M. Biodegradable materials for bone repair and tissue engineering applications. *Materials*. 2015;8:5744-5794.
17. Wei S, Ma J-X, Xu L, Gu X-S, Ma X-L. Biodegradable materials for bone defect repair. *Mil Med Res*. 2020;7:54.
18. Gao C, Peng S, Feng P, Shuai C. Bone biomaterials and interactions with stem cells. *Bone Res*. 2017;5:1-33.
19. Gu M, Liu Y, Chen T, et al. Is graphene a promising Nano-material for promoting surface modification of implants or scaffold materials in bone tissue engineering? *Tissue Eng Part B Rev*. 2014;20:477-491. doi:10.1089/ten.teb.2013.0638
20. Rana K, Ghosh R, Rawat NK. 2D graphene nanostructures for biomedical applications. *Monoelements*. John Wiley & Sons, Ltd; 2020:261-284. doi:10.1002/9781119655275.ch10
21. Bahrami S, Baheiraei N, Shahrezaee M. Biomimetic reduced graphene oxide coated collagen scaffold for in situ bone regeneration. *Sci Rep*. 2021;11:16783.
22. Mahanta AK, Patel DK, Maiti P. Nanohybrid scaffold of chitosan and functionalized graphene oxide for controlled drug delivery and bone regeneration. *ACS Biomater Sci Eng*. 2019;5:5139-5149.
23. Cheng X, Wan Q, Pei X. Graphene family materials in bone tissue regeneration: perspectives and challenges. *Nanoscale Res Lett*. 2018;13:289.
24. Shin YC, Song S-J, Jeong SJ, et al. Graphene-based nanocomposites as promising options for hard tissue regeneration. In: Chun HJ, Park CH, Kwon IK, Khang G, eds. *Cutting-Edge Enabling Technologies for Regenerative Medicine*. Springer; 2018:103-117. doi:10.1007/978-981-13-0950-2_6
25. Arnold AM, Holt BD, Daneshmandi L, Laurencin CT, Sydlik SA. Phosphate graphene as an intrinsically osteoinductive scaffold for stem cell-driven bone regeneration. *Proc Natl Acad Sci*. 2019;116:4855-4860.
26. Pan S, Yin J, Yu L, et al. 2D MXene-integrated 3D-printing scaffolds for augmented osteosarcoma phototherapy and accelerated tissue reconstruction. *Adv Sci*. 2020;7:1901511.
27. Zhang J, Fu Y, Mo A. Multilayered titanium carbide MXene film for guided bone regeneration. *Int J Nanomedicine*. 2019;14:10091-10103.
28. Chen K, Chen Y, Deng Q, et al. Strong and biocompatible poly(lactic acid) membrane enhanced by Ti3C2Tz (MXene) nanosheets for guided bone regeneration. *Mater Lett*. 2018;229:114-117.
29. Rasool K, Mahmoud KA, Johnson DJ, Helal M, Berdiyorov GR, Gogotsi Y. Efficient antibacterial membrane based on two-dimensional Ti3C2Tx (MXene) nanosheets. *Sci Rep*. 2017;7:1598.
30. Dwivedi N, Dhand C, Kumar P, Srivastava K. Emergent 2D materials for combating infectious diseases: the potential of MXenes and MXene–graphene composites to fight against pandemics. *Mater Adv*. 2021;2:2892-2905.
31. Arabi Shamsabadi A, Sharifian Gh M, Anasori B, Soroush M. Antimicrobial mode-of-action of colloidal $Ti_3C_2T_x$ MXene nanosheets. *ACS Sustain Chem Eng*. 2018;6:16586-16596.
32. Zamhuri A, Lim GP, Ma NL, Tee KS, Soon CF. MXene in the lens of biomedical engineering: synthesis, applications and future outlook. *Biomed Eng Online*. 2021;20:33.
33. Zheng K, Li S, Jing L, Chen P-Y, Xie J. Synergistic antimicrobial titanium carbide (MXene) conjugated with gold nanoclusters. *Adv Healthc Mater*. 2020;9:2001007.
34. Gogotsi Y, Anasori B. The rise of MXenes. *ACS Nano*. 2019;13:8491-8494.
35. Limbu TB, Kumari S, Wang Z, et al. Ingeniously enhanced ferromagnetism in chemically-reduced 2D Ti3C2TX MXene. *Mater Chem Phys*. 2022;285:126155.
36. Limbu TB, Chitara B, Orlando JD, et al. Green synthesis of reduced $Ti_3C_2T_x$ MXene nanosheets with enhanced conductivity, oxidation stability, and SERS activity. *J Mater Chem C*. 2020;8:4722-4731.
37. Limbu TB, Chitara B, Garcia Cervantes MY, et al. Unravelling the thickness dependence and mechanism of surface-enhanced Raman scattering on $Ti_3C_2T_x$ MXene nanosheets. *J Phys Chem C*. 2020;124:17772-17782.
38. Peters JP, Van Slyke, DD: Quantitative clinical chemistry, vol 2,williams and wilkins, Baltimor (MD),1932, 760.
39. Tietz NW. Blood gases and electrolytes. In:Fundamentals of clinical chemistry. NW tietz, editor,Saunders, Philadelphia, 176, 903–908.
40. Young DS. *Effects of drugs on clinical laboratory tests*. AACC press; 1990.
41. Thermo Fisher Scientific. Piper Phosphate Assay Kit. https://tools.thermofisher.com/content/sfs/manuals/mp22061.pdf. Retrieved May 31 2024.
42. Gomes A, da Silva F, Eckhart KE, Matiuzzi da Costa M, Sydlik SA, Pequeno de Oliveira H. Inhibition of biofilm formation induced by functional graphenic materials impregnated in Nile tilapia (Oreochromis niloticus) skin. *Appl Surf Sci*. 2022;576:151768.
43. E. Eckhart K, M. Arnold A, A. Starvaggi F, A. Sydlik S. Tunable, bacterio-instructive scaffolds made from functional graphenic materials. *Biomater Sci*. 2021;9:2467-2479.
44. McBeath R, Pirone DM, Nelson CM, Bhadriraju K, Chen CS. Cell shape, cytoskeletal tension, and RhoA regulate stem cell lineage commitment. *Dev Cell*. 2004;6:483-495.
45. Hart NH, Nimphius S, Rantalainen T, Ireland A, Siafarikas A, Newton RU. Mechanical basis of bone strength: influence of bone material, bone structure and muscle action. *J Musculoskelet Neuronal Interact*. 2017;17:114-139.
46. Kim SB, Kim YJ, Yoon TL, et al. The characteristics of a hydroxyapatite–chitosan–PMMA bone cement. *Biomaterials*. 2004;25:5715-5723.
47. Webb JCJ, Spencer RF. The role of polymethylmethacrylate bone cement in modern orthopaedic surgery. *J Bone Joint Surg Br*. 2007;89-B:851-857.

SUPPORTING INFORMATION

Additional supporting information can be found online in the Supporting Information section at the end of this article.

How to cite this article: Orlando JD, Li L, Limbu TB, et al. Calcium phosphate graphene and $Ti_3C_2T_x$ MXene scaffolds with osteogenic and antibacterial properties. *J Biomed Mater Res*. 2024;112(6):e35434. doi:10.1002/jbm.b.35434